chromatin, these x-ray images of rat sperm nuclei have also demonstrated that x-ray lasers can resolve structures as small as 500 Å attached to biological structures. Whereas additional studies must be performed to refine the estimates of tightly bound water in sperm chromatin provided by these images, these results support recent AFM studies that show that sperm chromatin must be extensively hydrated. This water of hydration, which may contribute as much as one-third of the volume of the rat sperm nucleus, is most likely located within the 600 to 1000 Å nodules of sperm chromatin (*12*) and between lamellae (*13, 14*).

An advantage of x-ray microscopy that will prove useful in future studies is that it can also be used to obtain information about elemental density. By selecting an appropriate x-ray laser wavelength, one can enhance the contrast between elements. In Fig. 3, we show the wavelengths of demonstrated nickel-like x-ray lasers along with the calculated transmission for 1 μm of water, DNA, and protein and for 500 Å of gold. The large change in absorption across the carbon absorption edge at 44.3 Å can be used to map out carbon abundance when two images of the specimen are taken, one with the tantalum x-ray laser (44.83 Å wavelength) and one with the tungsten x-ray laser (43.8 Å wavelength). Such data obtained for rat sperm nuclei, for example, would provide the additional information we need to better estimate the extent of sperm chromatin hydration.

The 44.83 Å wavelength of the nickel-like tantalum x-ray laser used in these experiments is nearly optimal for the imaging of biological specimens that have been immunogold-labeled. The development of normal incidence multilayer x-ray optics at wavelengths below the carbon K-edge (43.7 Å), where there is high contrast between proteins and water, will make short wavelength x-ray laser microscopes possible. Theoretical calculations indicate that short wavelength x-ray optics can be fabricated with existing technology, and we expect several groups to succeed within a year. In addition, improvements in the capability of current x-ray lasers through the use of multilayer mirrors to double-pass the gain region or through increasing the laser gain should lead to 100 to 1000 times more output. The increase in energy will allow combining several microscopes to produce images of the object along different lines of sight. These multiple frames could be synchronized to obtain three-dimensional images or time-delayed to observe the effects of high dosage on specimens. In addition, new glass laser technology affording high average power should allow the construction of x-ray lasers that are more compact (3 by 10 m) than the Nova laser and cost less ($1 million rather than several hundred million dollars) and that offer reasonable repetition rates (once every 5 to 10 min) (*18*).

REFERENCES AND NOTES

1. C. Jacobsen *et al.*, *Opt. Commun.* **86**, 351 (1991).
2. W. Meyer-Ilse *et al.*, in *X-Ray Microscopy III*, A. Michette, G. Morrison, C. Buckley, Eds. (Springer-Verlag, Berlin, 1991), pp. 284–289.
3. T. Tomie *et al.*, *Science* **252**, 691 (1991).
4. C. H. Skinner *et al.*, *J. Microsc.* **159**, 51 (1990).
5. B. J. MacGowan *et al.*, in *X-Ray Lasers 1990*, G. J. Tallents, Ed. (IOP Publishing, York, United Kingdom, 1990), pp. 221–230.
6. L. B. DaSilva *et al.*, *Opt. Lett.* **17**, 754 (1992).
7. B. J. MacGowan *et al.*, *Phys. Rev. Lett.* **65**, 420 (1990).
8. E. Anderson and D. Kern, in *X-Ray Microscopy III*, A. Michette, G. Morrison, C. Buckley, Eds. (Springer-Verlag, Berlin, 1991), pp. 75–78.
9. M. D. Rosen *et al.*, *Phys. Rev. Lett.* **54**, 106 (1985).
10. T. W. Barbee, *Opt. Eng.* **29**, 581 (1990).
11. G. B. Dooher and D. Bennett, *Am. J. Anat.* **136**, 339 (1973).
12. M. J. Allen, G. C. Pogany, W. Siekhaus, R. Balhorn, *J. Cell Biol.* **111**, 110 (1990).
13. J. K. Koehler, *J. Ultrastruct. Res.* **33**, 598 (1970).
14. J. Koehler, U. Wurschmidt, M. P. Larsen, *Gamete Res.* **8**, 357 (1983).
15. R. Balhorn, B. L. Gledhill, A. Wyrobek, *Biochemistry* **16**, 4704 (1977).
16. The protamine-DNA complex consists of 1 molecule of protamine to 10 bp of DNA and is designated by the formula $C_{477}H_{757}O_{179}N_{214}P_{20}S_9$.
17. M. J. Allen *et al.*, *J. Cell Biol.* **115**, 50 (1991).
18. J. T. Hunt, in *Solid State Lasers II*, G. Dube, Ed. [Society of Photo-Optical Instrumentation Engineers (SPIE) proceedings, Los Angeles, 1991], vol. 1410, pp. 2–14.

19. The authors are indebted to J. Kilkenny, M. Eckart, R. Stewart, and the Nova Experiments Group for support and assistance. We would also like to thank J. Cox, R. Wing, M. Carter, R. Levesque, F. Kelly, D. Montgomery, and G. Shimkaveg for their contributions. Supported by U.S. Department of Energy Office of Health and Environmental Research and performed under the auspices of the U.S. Department of Energy by the Lawrence Livermore National Laboratory under contract W-7405-ENG-48. The work at the Lawrence Berkeley Laboratory is supported by the U.S. Department of Energy Office of Basic Energy Sciences and the Air Force Office of Scientific Research.

12 June 1992; accepted 13 August 1992

Room-Temperature, Electric Field–Induced Creation of Stable Devices in CuInSe$_2$ Crystals

David Cahen,* Jean-Marc Gilet, Claus Schmitz,† Leonid Chernyak, Konstantin Gartsman, Abram Jakubowicz‡

Multiple-junction structures were formed, on a microscopic scale, at room temperature, by the application of a strong electric field across originally homogeneous crystals of the ternary chalcopyrite semiconductor CuInSe$_2$. After removal of the electric field, the structures were examined with electron beam–induced current microscopy and their current-voltage characteristics were measured. Bipolar transistor action was observed, indicating that sharp bulk junctions can form in this way at low ambient temperatures. The devices are stable under normal (low-voltage) operating conditions. Possible causes for this effect, including electromigration and electric field–assisted defect reactions, are suggested.

The use of semiconductors in devices depends critically on our ability to tailor their electronic properties. This is achieved chemically by doping, which is the controlled introduction of species different from those making up the semiconductor. The dopants are usually foreign species and they are introduced by thermal diffusion or ion implantation. Both are high-energy processes. We have found that controlled, local changes in the concentrations of dopants can be made, at ambient temperature, in ternary chalcogenide semiconductors, especially CuInSe$_2$, without the introduction of any foreign species, as a result of the action of strong electric fields (*E* fields). The process is illustrated by the formation of bipolar transistor structures.

The use of *E* fields to change preexisting doping profiles obtained by thermal diffusion goes back to the early days of Si and Ge semiconductor science (*1, 2*). Indeed, the compensated material needed for the action of Si:Li detectors is obtained by controlled electromigration of Li after its thermal indiffusion into Si (*3*). The so-called "forming" of contacts to Se rectifiers has also been related to dopant electromigration (*4*). Other examples of the action of *E* fields on semiconductor doping include deep-level defect gettering in Si, Ge, or GaAs (*5–7*).

The relative ease by which CuInSe$_2$ (CISe) can be doped to yield *n*- or *p*-type CISe has been ascribed to its doping by native defects (*8*) (although doping by foreign species is possible as well). Thus diodes have been formed in originally *p*-CISe by thermal indiffusion of Cu or In (*9, 10*); facile homojunction formation was observed in single-crystal CISe as a result of

---

Department of Materials and Interfaces, Weizmann Institute of Science, Rehovot, Israel.

*To whom correspondence should be addressed.
†Present address: Institut für SOLARE Energieversorgungstechnik, Kassel, Germany.
‡Present address: IBM Research Laboratories, Rüschlikon, Switzerland.

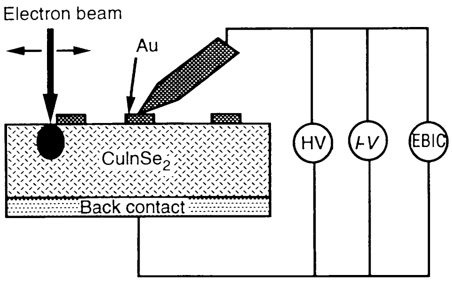

Fig. 1. Schematic of the experimental setup, showing the point contact and (optional) small-area Au (or Pt) dot contacts, the scanning electron beam, and the volume in which electron-hole pairs are created, as a result of the beam (*24*). High voltage (HV) can be applied and current-voltage characteristics (*I-V*) and EBIC can be measured, as shown.

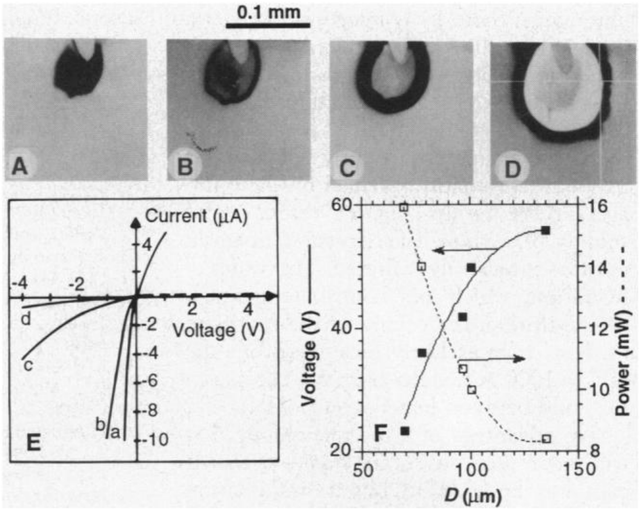

Fig. 2. EBIC images of the surface of a *p*-CuInSe$_2$ crystal, with an evaporated Au contact on it. Sample characteristics: Cu:In:Se = 22.6:26.6:50.8 atom %; electrical resistivity $\rho \approx 4.5 \times 10^3$ ohm-cm; Hall mobility $\mu \approx 10$ cm^2 V^{-1} s^{-1} [net concentration of electronic carriers (holes) $\approx 1.5 \times 10^{14}$ cm^{-3}]. Experimental conditions for EBIC: beam voltage, 30 kV; spot size, 100 nm; beam current, ≈1 nA; white contrast corresponds to the flow of electrons from the top contact into the bulk. **(A)** Before application of positive bias to the Au contact, showing only a metal-semiconductor barrier (corresponds to the *I-V* characteristic as in curve a in (E); the high resistance in the forward direction is due to the low (original) carrier concentration of the crystal). **(B)** After application of positive bias (36 V, 78 min, 50% duty cycle triangular pulses at 100 Hz) to the Au contact, showing the formation of a junction outside the area of the Au contact (corresponds to the *I-V* characteristic in curve b in (E), which shows an increase in the forward resistance). **(C)** After application of further positive bias [50 V, 98 min, same wave form as in (B)] to the Au contact, showing the disappearance of contrast near the metal contact (corresponds to the *I-V* characteristic in curve c in (E), which shows further increase in the forward resistance). **(D)** After application of still further positive bias to the Au contact [56 V, 138 min, same wave form as in (B)], showing the formation of a second junction (corresponds to the *I-V* characteristic in curve d in (E), with blocking behavior in both directions). The cross hairs show the spot for electron beam excitation of the sample, to obtain the *I-V* curves of Fig. 4. **(E)** Time evolution of *I-V* curves, measured during the experiment, before, between, and after high-voltage biasing. The maximum voltages that were applied for the *I-V* measurements were lower (≤4 V) than the voltages used to create the desired structures. Curves a to d correspond to EBIC images (A) through (D) (see below). The dashed line shows, schematically, the blocking (reverse bias) parts of curves b, c, and d. Positive polarity corresponds to the top contact positive with respect to the back contact. **(F)** Dependence of the extent of the ring-like EBIC contrast, as shown in (B), (C), and (D), on applied voltage and on the *I-V* product. *D*, diameter of most external region of contrast.

vacuum deposition of CdS or Cd (*11*). In all these cases an external chemical phase is involved. In the experiments reported here, bulk microscopic homojunctions are formed in originally homogeneous material after an *E* field is applied to it, by means of point or small-area metal contacts. Although the actual mechanisms are not completely clear, the successful demonstration of two-terminal bipolar phototransistor action shows the dramatic effects that can be obtained. Conventional preparation of a thin-film transistor with polycrystalline thin-film *p*-CISe, a material that is under intensive investigation for use in photovoltaic devices (*12*), has been reported (*13*).

The semiconductor CuInSe$_2$ with an optical bandgap, E_G, of 1.02 eV (at room temperature) has the ordered zincblende, chalcopyrite ($I\bar{4}2d$) structure. We show elsewhere that, in addition to *p*- or *n*-type semiconductivity, this material can exhibit some ionic conductivity as a result of Cu mobility (*14*). This semiconductor differs from normal mixed conductors in that it shows respectable semiconducting properties (the samples for which we report results here had net hole concentrations of 10^{13} to 10^{14} cm^{-3} and Hall mobilities of 100 to 10 cm^2 V^{-1} s^{-1}) and in that a gradient of the chemical potential of the mobile species can exist in it, in the absence of an applied electrical potential. We have termed materials with such a combination of properties "semionics" (*15*). Using a point-contact potentiostatic current decay method (*16*), we measured effective chemical diffusion coefficients of Cu in the samples, at room temperature, and found relatively high values ($\geq 10^{-8}$ cm^2 s^{-1}). These observations fit with the vacancy diffusion mechanism that we propose (*14*), because the samples are Cu-poor. Elsewhere we show that such measurements can lead to a systematic overestimate of two to four orders of magnitude, due to uncertainty about the actual contact area [see the discussion in the appendix of (*14*)]. This is important because otherwise it is not possible to explain the observed stability of the doping profiles and the device action (see below). Samples with compositions closer to stoichiometry had smaller effective values by up to four orders of magnitude (*14*). Although we did succeed in making device-like structures in them (*17–20*), they were, in general, more difficult to work with.

Single crystals, used for the results reported here, were grown for the National Renewable Energy Laboratory (Golden, Colorado) by K. J. Bachmann, by direct solidification of near-stoichiometric melts, under a Se pressure of 10^3 Pa (*21*). Similar results can be obtained on other samples, including (Cu,Ag)InSe$_2$ samples grown by us (*22*). Front contacts were either ≤25 μm in diameter, mechanically sharpened Au or Pt points, placed directly on the polished and etched (in Br$_2$-methanol solution) CISe surface, or 50 μm in diameter, evaporated Au spots, 10 to 20 nm thick (Fig. 1). Typical sample thicknesses were 0.5 mm. All of the back side (3 to 4 mm^2) was used for (evaporated Au) back contact. The experiments were performed inside a Philips 515 scanning electron microscope (SEM), modified for electron beam-induced current (EBIC) and with the possibility for placing the top contact onto the sample at predetermined positions. This configuration resulted in weak Schottky barriers between the sample and the top contact (0.3 to 0.4 eV), giving an EBIC signal just under the Au spot [see (*11*)]. The main parameter that was varied was the time-voltage profile. The voltage was applied in the reverse direction to obtain high *E*-field strengths locally. The bias was slowly increased until the current started to increase steeply (close to reversible breakdown of the avalanche type), and care was taken to avoid (irreversible) thermal breakdown. This process was repeated, with steadily increasing voltage needed for current increase, until no further changes in the current-voltage (*I-V*) relation and EBIC resulted (Fig. 2, A through E).

For the *I-V* measurements (Fig. 2E) the maximum voltages that were applied were maintained well below the voltages used to create the desired structures (Fig. 2, A through D). In Fig. 2E, curve a is the initial characteristic of the metal-semiconductor contact. Application of a sufficiently high *E* field in the reverse direction (to modify the

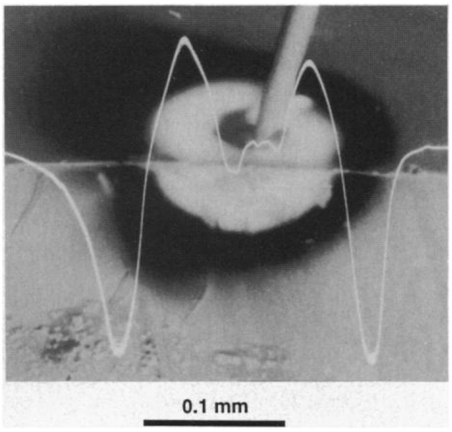

Fig. 3. Mixed EBIC and secondary electron (SE) image, plus superimposed EBIC line scan (taken through the center of the structure, on the top surface), of a *p*-CuInSe$_2$ sample, after the application of an electrical bias of 200 V, trapezoidal pulses at 45 Hz (~45% duty cycle) for 5 min. The sample was cleaved after this, yielding the view shown with the cleavage plane in the lower half of the image. Contact to the evaporated Au spot on the top surface (upper half of the image) is made by an Au wire. Experimental conditions for EBIC/SE are as in Fig. 2.

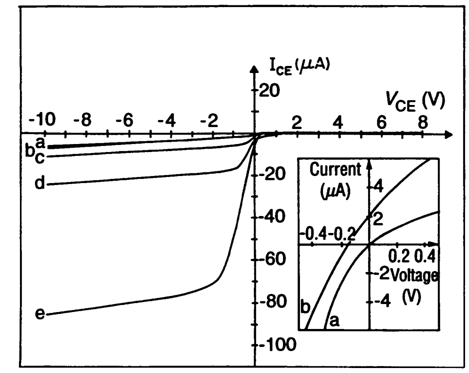

Fig. 4. Plot of the *I-V* characteristics obtained with the structure corresponding to Fig. 2D and curve d in Fig. 2E, by exciting the external junction of the structure with the electron beam. The beam current was changed by varying the spot size, from (curve a) 0 nA (dark, that is, without electron beam excitation) to (curve b) 0.25 nA (50 nm) to (curve c) 0.9 nA (100 nm) to (curve d) 3.2 nA (300 nm) to (curve e) 16.7 nA (500 nm). The beam currents were measured by means of a Faraday cup. Absorbed currents were, as a rule, 60% of the measured beam currents. Polarity was as in Fig. 2E. (Inset) Curve b: same, but for the structure of Fig. 2A, with 500-nm (16.7 nA) electron beam spot size; curve a: without the electron beam (same as curve a in Fig. 2E), and shown for comparison only; CE, collector-emitter.

material) led to a continuous increase of the resistance (Fig. 2E, curves b and c, forward direction). Finally a situation was reached where blocking was observed for both voltage polarities (Fig. 2E, curve d). Application of high fields in the forward direction did not lead to changes, until thermal breakdown.

Initially all modifications of the semiconductor were confined to a shallow region below its surface (as confirmed by junction EBIC results), where the material is depleted of charge carriers as a result of the reverse direction of the applied *E* field (Fig. 2A). Subsequently the *E* field induced permanent changes as expressed by the formation of an internal *E* field, surrounding the metal contact (compare Fig. 2, B and C, with Fig. 2A, obtained before application of the *E* field). We interpret this, in view of the *I-V* curves, as due to local changes in carrier concentration, leading to the formation of a *p-n* junction positioned outside the area covered by the contact (EBIC reveals a ring; Fig. 2, B and C). Seebeck coefficient measurements confirmed the conversion from one type of conductivity to another below the metal. Further treatment resulted in the formation of a second junction, as shown by EBIC (Fig. 2D). The dependences of the extent of the effect on the applied voltage and on the power needed are shown in Fig. 2F. The dependence of the EBIC signal on the electron beam voltage, junction EBIC measurements near an edge, as well as EBIC measurements on samples, cleaved after application of the *E* field (Fig. 3), show that these features can extend up to hundreds of micrometers into the material.

Secondary ion mass spectroscopy of structures, after *E*-field application, shows that Au from the contact penetrates at the most a few micrometers (*23*). No changes could be observed in the backscattered electron imaging modes of the SEM, but with secondary electron imaging voltage contrast was seen, which could be compensated for by small (≤0.5 V) external voltages. Control over this process is shown by the fact that we could produce repeatedly the same structure on different areas of the same surface; however, although the process is reversible in its initial stages, once a complete structure is formed, it cannot be changed except by catastrophic breakdown. These results were obtained without any evidence for Cu^0 precipitation under or near the contact, even though the reverse bias had the correct polarity for this. At no stage did we see any evidence for melting of the semiconductor or of the contact; the same was also true when metals of lower melting point, such as Al, Cd, and In, were used.

Because the final configuration consists of two junctions in series (Fig. 2D), it represents the basic structure of a bipolar transistor. The presence of two junctions is consistent with the bipolar blocking behavior of the final *I-V* curve (Fig. 2E, curve d). One way to prove that relatively sharp (bulk) junctions are formed is to check to see if this structure behaves as a (bipolar) transistor. To do this, we operated it in the two-terminal phototransistor mode, using the top and bottom contacts that served to create the device as emitter and collector. This was done to avoid possible point contact transistor action that can result when a second small area contact is made to the middle ("base") region. Because the experiments were performed in the SEM, we used electrons (instead of photons) to generate excess carriers.

Figure 4 shows the *I-V* curves obtained under electron beam excitation, on the original metal contact (inset, curve b) and on the final transistor-like structure. Without changing the measuring configuration and only as a result of the action of the *E* field, the effect of electron beam excitation shifts from the upper left quadrant of the *I-V* plot to the lower left one (or to the upper right one, depending on the area excited by the electron beam). The nonlinearity of the curves in Fig. 4 is typical for transistor behavior. To calculate amplification, we use the EBIC efficiency, expressed as a generation factor, G, by

$$G = I_{EBIC}/I_e \qquad (1)$$

where I_e is the number of electrons per second deposited in the sample by the electron beam, the absorbed current. For our samples I_e was 0.6 to 0.7 times the beam current, as measured by a Faraday cup. The theoretical maximum of G (for 30-keV electrons), on the basis of the beam current (*24*), is

$$30{,}000/E_G \times 3.3\ (\approx 9000) \qquad (2)$$

With absorbed instead of beam current this value decreases to ≈6000. We find a dramatic increase in G from ≈1000 (for the initial metal contact) up to ≈5500. We ascribe this relatively low value to the presence of a high dark, leakage current (Fig. 4, curve a) in our structures. This is so not only because of the quality of the material but also because of the high injection conditions, which decrease the absolute generation efficiency of the electron-hole pair. Evidence for amplification was found in device structures, obtained in similar CISe and (Cu,Ag)InSe$_2$ samples, with either point or evaporated Au contacts, for which the relative increase of device response with increasing electron beam current was much higher than the corresponding relative increase of the electron beam current. Thus, an increase of the electron beam current by 40% increased the device response by 450%. Such behavior cannot be due to a photodiode effect only. Thus, the *I-V* curves, both those measured without and those measured with electron beam excitation, together with the EBIC observations and the hot probe results, demonstrate the formation of multiple junctions in the bulk of the material by the application of *E* fields. The device response indicates that these junctions are relatively sharp.

A number of explanations, to be discussed in detail elsewhere (*20, 22*), can be given for these observations, namely, thermal effects, *E* field–induced defect reactions (creation or annihilation, dissociation or association of defects) and electromigration of defects. All involve local changes in the concentration of doping defects, something for which we obtained indirect evidence from changes in the intensity and energy of peaks in cathodoluminescence spectra. Major problems that any model to explain our observations must address are the stability of the changes and the ability to form two junctions of opposite polarity without changing the polarity of the bias voltage.

The regularity shown in Fig. 2, A through D, suggests the occurrence of electromigration, but the stability of the changes (why do the dopants not diffuse back in the electrochemical potential gradient?) argues against this, unless *E*-field application leads to a local decrease in the chemical diffusion coefficient [by a change in the thermodynamic factor (*25*) or jump frequency (*26, 27*), such as through a change in vacancy concentration]. In addition, the single junction, observed first (by EBIC), indicates a decrease in the concentration of acceptors (or an increase in the concentration of donors) near the small area anode (with correspondingly opposite results for *n*-type samples), that is, apparent counter-Coulombic effects. We can offer two possible explanations for this latter observation.

1) Formation of an ion migration "wake," the formation of a trough and a crest in the concentration of the mobile dopant, where the junction due to the trough is initially "shadowed" by the junction due to the crest and only becomes observable when further migration, away from the contact, occurs. In some instances we have been able to observe such a situation by using EBIC under bias and have seen indications for it in *I-V* characteristics. In this case the Coulomb force, $\mathbf{F}_d = Z_d q \mathbf{E}$ [where Z_d is the (effective) valence of the migrating defect, q is the electron charge, and $\mathbf{E}$ is the *E* field], can explain our observations.

2) Electron "wind" can explain the apparent counter-Coulombic charge flow, indicated by the polarity reversal of the innermost junction. It exerts a force $\mathbf{F}_w = -n_e \lambda_e s_e q \mathbf{E}$, where n_e is the density of electronic carriers, λ_e is the mean free path between scattering events, and s_e is the cross section for electron-ionized impurity scattering. Comparing $\mathbf{F}_d$ and $\mathbf{F}_w$, we see that the wind effect will dominate only if $(n_e \lambda_e s_e) > Z_d$. The wind (or "drag") effect, well known in metal physics (*28*), causes migration of atoms or ions as a result of the transfer of momentum from electronic carriers to them. This can be possible during the current spikes, achieved during the momentary (avalanche) breakdown that often accompanies the changes in EBIC. Its opposite polarity can explain why no Cu^0 precipitation is observed.

Because we work in reverse bias, the possibility of recombination–enhanced defect reactions (*29*) is low. However, during avalanche, when chemical bonds will be weakened in the junction region, a mechanism such as SLEF (short-lived large energy fluctuations) (*30*) can be operative. It is also possible that the *E* field acts directly by changing locally the Fermi energy, thus changing the charge state of defects (*31*). On a larger scale, dislocations and grain boundaries can act as a source or trap for dopants. We have observed a strong correlation between the EBIC profile and chemical etch pits in similar experiments on (Cd,Hg)Te (*32*).

The observation that both high voltages and (transient) high currents are needed to produce these stable devices (Fig. 2F) suggests that localized heating effects do play a role, albeit a limited one, because no melting occurs. These effects are expected to be strongest around junctions, owing to the injection of hot carriers and electron-phonon interactions. They can locally enhance the diffusion of defects or defect reactivity. The relative sharpness of the EBIC signal can then be explained by the nonequilibrium nature of the process, that is, the momentary presence of high currents, leading to thermal spikes, and thus to effects akin to rapid thermal annealing. Because the phenomenon described here occurs under conditions of high excitation, it is likely that a combination of these effects is responsible for its observed stability and regularity; for instance, the occurrence of SLEFs may activate a fast ionic transport mechanism (*33*).

In conclusion, we have shown that room-temperature application of external *E* fields to CISe crystals can lead to local type conversion and to the creation of bulk junctions, without the introduction of a foreign phase and without melting of sample or contact. Such junctions are stable after removal of the *E* field and sufficiently sharp to permit device action. This suggests a "chimie douce" (soft chemistry, that is, at low temperature) way to control the local microcomposition and properties of such semiconductors and, possibly, a way to fabricate monolithic devices. Further scaling-down of the phenomenon, to achieve nanofabrication, appears technically feasible, with scanning-tunneling–or force microscope–like probes, possibly in a field-emission mode, to affect changes in the bulk under the surface on a nanometer scale.

REFERENCES AND NOTES

1. J. C. Severiens and C. S. Fuller, *Phys. Rev.* **92**, 1322 (1953).
2. C. S. Fuller and J. C. Severiens, *ibid.* **96**, 21 (1954).
3. E. M. Pell, *J. Appl. Phys.* **31**, 291 (1960).
4. M. I. El-Azab and C. H. Champness, *IEEE Trans. Electron Devices* **ED-27**, 253 (1980).
5. A. J. Tavendale, S. J. Pearton, A. A. Williams, D. Alexiev, *Appl. Phys. Lett.* **56**, 1457 (1990).
6. S. J. Pearton and A. J. Tavendale, *ibid.* **41**, 1148 (1982).
7. ———, *ibid.*, p. 176.
8. H. Neumann, *Cryst. Res. Technol.* **18**, 483 (1983).
9. R. D. Tomlinson, E. Elliott, J. Parkes, M. J. Hampshire, *Appl. Phys. Lett.* **26**, 383 (1975).
10. I. Shih, A. V. Shahidi, C. H. Champness, *J. Appl. Phys.* **56**, 421 (1984).
11. R. J. Matson, R. Noufi, K. J. Bachmann, D. Cahen, *Appl. Phys. Lett.* **50**, 158 (1987).
12. A. Rockett and R. W. Birkmire, *J. Appl. Phys.* **70**, R81 (1991).
13. J. Lai, L. Cai, D. L. Morel, *Appl. Phys. Lett.* **59**, 1990 (1991).
14. G. Dagan, T. Ciszek, D. Cahen, *J. Phys. Chem.* in press.
15. D. Cahen, in *Ternary and Multinary Compounds, Proceedings of the Seventh International Conference*, S. K. Deb and A. Zunger, Eds. (Materials Research Society, Pittsburgh, 1987), vol. TMC, p. 433.
16. H. Rickert and H. D. Wiemhöfer, *Solid State Ionics* **11**, 257 (1983).
17. A. Jakubowicz, G. Dagan, D. Cahen, *Bull. Isr. Phys. Soc.* **35**, 12 (1989).
18. D. Cahen, A. Jakubowicz, G. Dagan, U.S. and Israel Patent Applications (March 1989).
19. D. Cahen, A. Jakubowicz, C. Schmitz, *J. Electron. Mater.* **19**, 23 (1990).
20. A. Jakubowicz, G. Dagan, C. Schmitz, D. Cahen, *Adv. Mater.*, in press.
21. K. J. Bachmann, M. Fearheiley, Y. H. Shing, N. Tran, *Appl. Phys. Lett.* **44**, 407 (1984).
22. L. Chernyak, K. Gartsman, D. Cahen, in preparation.
23. These measurements were made by S. Asher, National Renewable Energy Laboratory, Golden, CO.
24. H. J. Leamy, *J. Appl. Phys.* **53**, R51 (1982).
25. W. Weppner, *Solid State Ionics* **32–33**, 466 (1989).
26. G. E. Murch and A. S. Nowick, Eds., *Diffusion in Crystalline Solids* (Academic Press, Orlando, FL, 1984).
27. H. Rickert, *Electrochemistry of Solids* (Springer, Berlin, 1982).
28. P. S. Ho and T. Kwok, *Rep. Prog. Phys.* **52**, 301 (1989).
29. L. C. Kimerling, *Solid State Electron.* **21**, 1391 (1978).
30. Y. L. Khait, J. Salzman, R. Beserman, *Appl. Phys. Lett.* **53**, 2135 (1988).
31. W. Walukiewicz, *ibid.* **54**, 2094 (1989).
32. K. Gartsman, L. Chernyak, J.-M. Gilet, R. Triboulet, D. Cahen, *Appl. Phys. Lett.*, in press.
33. M. Aniya, *Solid State Ionics* **50**, 125 (1992).

34. We thank the U.S.–Israel Binational Science Foundation, Jerusalem, for continuing support, the MINERVA Foundation for a fellowship (to C.S.), the Israeli Ministry of Science and Technology and the Israeli Ministry of Absorption for support (of K.G.), and H. Neumann for critical reading of the manuscript. D.C. thanks O. Stafsudd for seminal discussions. We thank S. Asher for making the secondary ion mass spectroscopic measurements.

11 May 1992; accepted 5 August 1992